CONTENTS

JOURNAL OF RARE EARTHS
Vol. 35 No. 2 (February 2017)

CONTENTS

INVITED REVIEW

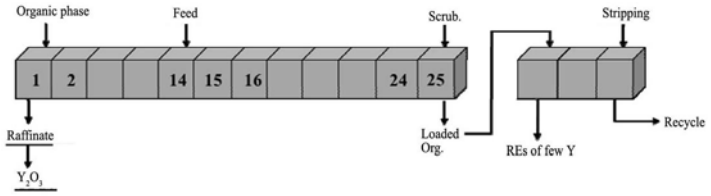

System	Organic phase	Feed	Scrub. acid
CA12-TBP	0.70 mol/L CA12 and 15%TBP, sapo-rate=90%	1.0 mol/L $RECl_3$	3.0 mol/L HCl
HAB-TBP	0.68 mol/L CA12, 0.12 mol/L C272 and 15%TBP, sapo-rate=90%	1.1 mol/L $RECl_3$	3.0 mol/L HCl

Separation process of Y with HAB

SPECTROSCOPY, LUMINESCENCE AND PHOSPHORS

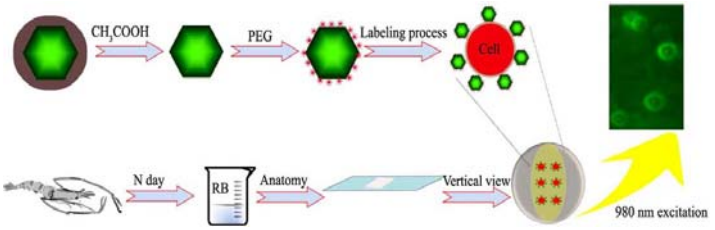

In vitro and in vivo bioimaging are carried out with shrimps using $NaREF_4$ (RE=0.4Y+0.4La+0.2(Yb,Er,Tm)) upconversion nanoparticles (UCNPs) as probes. The residual organic dye RB in shrimp can be detected on the basis of luminescent resonance energy transfer (LRET)

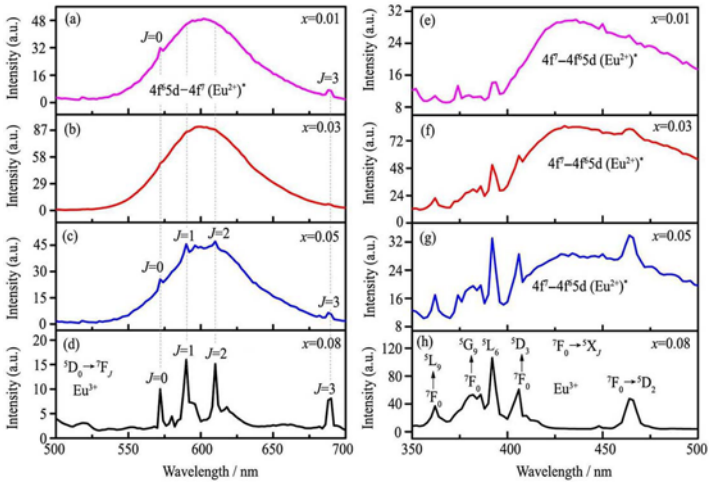

Emission (a–d) and excitation (e–h) spectra of the $(Sr_{1-x}Eu_x)_3Al_2O_6$ (x=0.01, 0.03, 0.05, and 0.08) phosphors synthesized with combustion-assisted solid-state reaction method

135 Synthesis and luminescent properties of $Ba_2V_2O_7:Sm^{3+}$

LI Fei, FANG Hongwei , CHEN Yonghu

J. Rare Earths, (35) 2017: 135-141

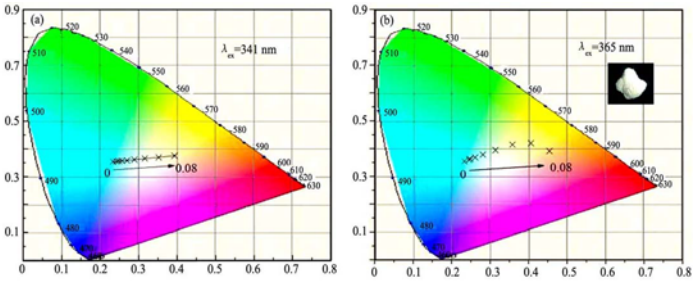

CIE chromaticity diagram for sample $Ba_2V_2O_7:xSm^{3+}$ (x=0.01, 0.02, 0.03, 0.04, 0.05, 0.06, 0.07 and 0.08, respectively) excited at 341 nm (a) and 365 nm (b) (The inset is the photograph of the $Ba_{1.95}V_2O_7:0.05Sm^{3+}$ powder excited at 365 nm)

142 Synthesis and luminescence of β-$SrGe(PO_4)_2$: RE (RE=Eu^{2+},Eu^{3+},Tb^{3+}) phosphors for UV light-emitting diodes

JIANG Yu, LIU Wei, CAO Xiyu, SU Ge, CAO Lixin, GAO Rongjie

J. Rare Earths, (35) 2017: 142-148

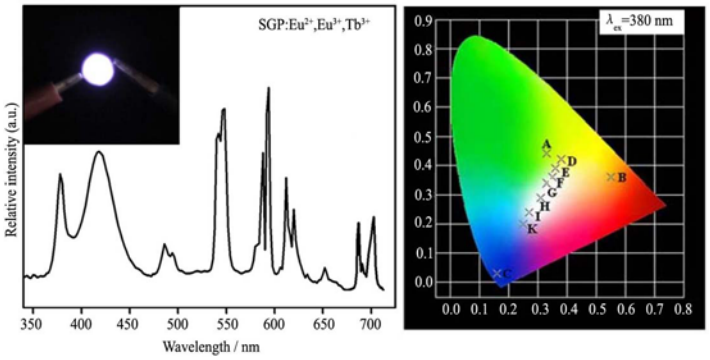

Electroluminescent spectra of the LED based on SGP:RE (RE=Eu^{2+}, Eu^{3+}, Tb^{3+}) phosphors (the inset shows the corresponding light image), and the CIE chromaticity coordinates of the mixed samples under 380 nm excitation

RARE EARTH CATALYSIS

149 Effect of high temperature pretreatment on the thermal resistance properties of $Pd/CeO_2/Al_2O_3$ close-coupled catalysts

HUANG Mulan, WANG Suning, LI Lan, ZHANG Hailong, SHI Zhonghua, CHEN Yaoqiang

J. Rare Earths, (35) 2017: 149-157

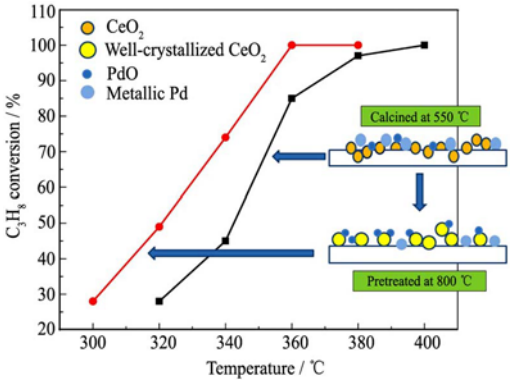

Improved catalytic performance of aged catalysts after 800 ℃ pretreatment

MAGNETISM AND MAGNETIC MATERIALS

158 Coercivity enhancement of Ce-Fe-B sintered magnets by low-melting point intergranular additive

CHEN Kan, GUO Shuai, FAN Xiaodong, DING Guangfei, CHEN Ling, CHEN Renjie, LEE Don, YAN Aru

J. Rare Earths, (35) 2017: 158-163

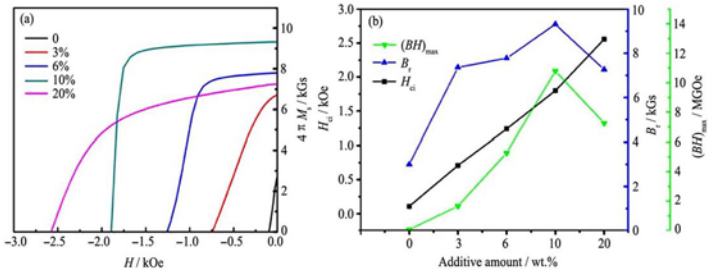

Demagnetization curves of $Ce_{17}Fe_{77}B_6$ with increasing Nd-based additive amounts (a) and the plot of magnetic properties of the $Ce_{17}Fe_{77}B_6$ magnet versus the increasing Nd-based additive amounts (b)

ADVANCED RARE EARTH MATERIALS

164 Chemical stability of Ce-doped zircon ceramics: Influence of pH, temperature and their coupling effects

XIE Yi, FAN Long, SHU Xiaoyan, CHI Fangting, DING Yi, MA Dengsheng, LU Xirui

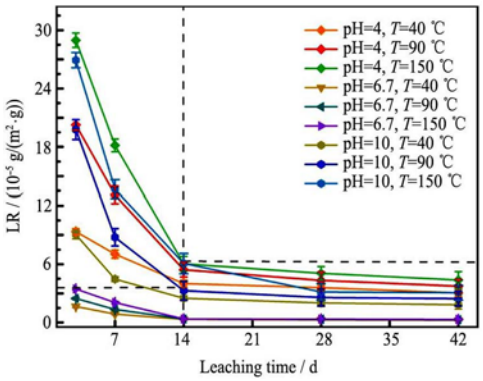

Normalized release rates of Ce in all discussed leachates

J. Rare Earths, (35) 2017: 164-171

172 Effect of CeO_2 on low temperature pressureless sintering of porous Si_3N_4 ceramics

LIU Tiantian, JIANG Cuifeng, GUO Wei

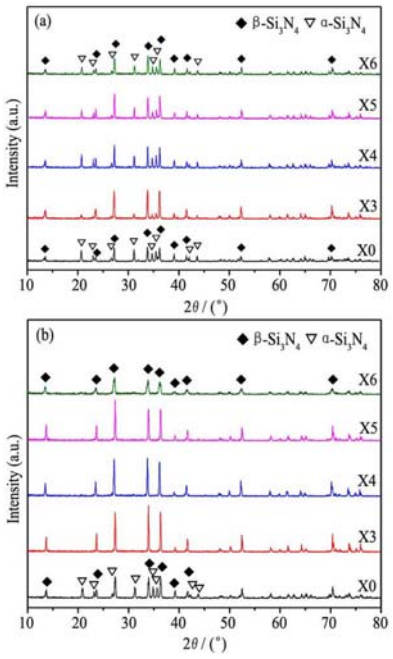

XRD patterns of Si_3N_4 ceramics at different temperatures
(a) At 1500 ºC; (b) At 1550 ºC

J. Rare Earths, (35) 2017: 172-176

CHEMISTRY AND HYDROMETALLURGY

177 Synthesis of ion imprinted polymers for selective recognition and separation of rare earth metals

Mashitah M. Yusoff, Nik Rohani Nik Mostapa, Md Shaheen Sarkar, Tapan Kumar Biswas, Md Lutfor Rahman, Sazmal Effendi Arshad, Mohd Sani Sarjadi, Ajaykumar D. Kulkarni

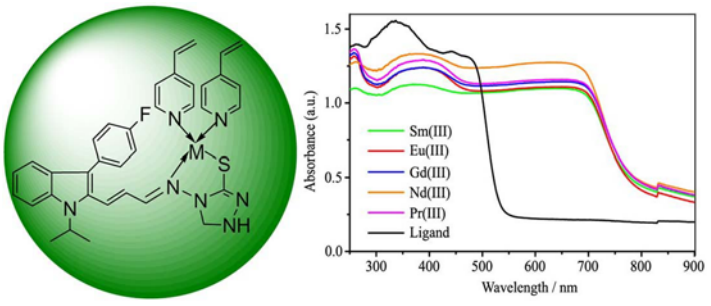

Schiff base lanthanide ion imprinted polymers (IIPs at left) and UV-vis absorption spectra for IIPs bind with lanthanide ions: Schiff base ligand (black line) and L-IIPs show various coloured line (right)

J. Rare Earths, (35) 2017: 177-186

187 *E*-pO^{2-} diagram for rare earth elements in molten salt

Yixing (Kevin) Shen, Jinsuo Zhang

J. Rare Earths, (35) 2017: 187-192

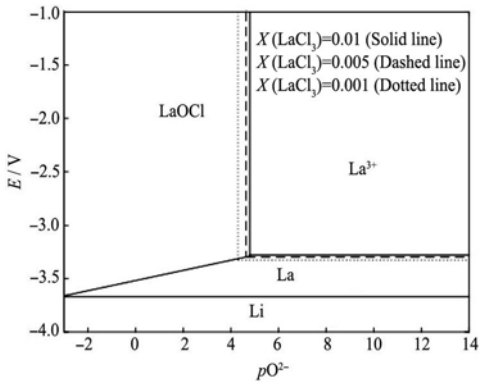

E-pO^{2-} diagram of La in eutectic LiCl-KCl melt at 723 K

193 Effect of combinative addition of mischmetal and titanium on the microstructure and mechanical properties of hypoeutectic Al-Si alloys used for brazing and/or welding consumables

WANG Bo, XUE Songbai, WANG Jianxin, LIN Zhongqiang

J. Rare Earths, (35) 2017: 193-202

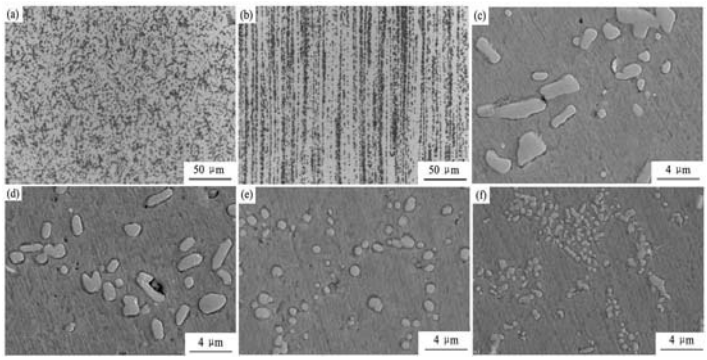

Microstructures of hot-extruded AST-*x*RE welding rods
(a) *x*=0.05, cross-sectional metallographic structure; (b) *x*=0.05, longitudinal-sectional metallographic structure; (c) *x*=0, cross-sectional SEM structure; (d) *x*=0.01, cross-sectional SEM structure; (e) *x*=0.05, cross-sectional SEM structure; (f) SEM microstructure of hot-extruded AST-0.02Sr welding rod for comparison

203 *In situ* observation of austenite grain growth and transformation temperature in coarse grain heat affected zone of Ce-alloyed weld metal

YAN Ning, YU Shengfu, CHEN Ying

J. Rare Earths, (35) 2017: 203-210

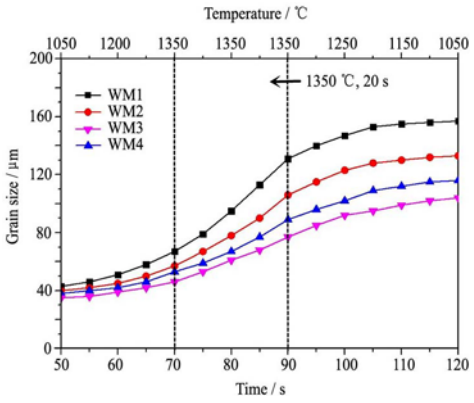

Change in the average austenite grain size with the increase of high-temperature residence time